
Incremental Learning and Self-Attention Mechanisms Improve Neural System Identification

Isaac Lin

Carnegie Mellon University
isaacl@cs.cmu.edu

Tianye Wang

Peking University
wangtianye17@pku.edu.cn

Shang Gao

Massachusetts Institute of Technology
shang111@mit.edu

Shiming Tang

Peking University
tangshm@pku.edu.cn

Tai Sing Lee

Carnegie Mellon University
tai@cnbc.cmu.edu

Abstract

Convolutional neural networks (CNNs) have been shown to be the state-of-the-art approach for modeling the transfer functions of visual cortical neurons. Cortical neurons in the primary visual cortex are sensitive to contextual information mediated by extensive horizontal and feedback connections. Standard CNNs can integrate global spatial image information to model such contextual modulation via two mechanisms: successive rounds of convolutions and a fully connected readout layer. In this paper, we find that non-local networks or self-attention (SA) mechanisms, theoretically related to context-dependent flexible gating mechanisms observed in the primary visual cortex, improve neural response predictions over parameter-matched CNNs in two key metrics: tuning curve correlation and tuning peak. We factorize networks to determine the relative contribution of each context mechanism. This reveals that information in the local receptive field is most important for modeling the overall tuning curve, but surround information is critically necessary for characterizing the tuning peak. We find that self-attention can replace subsequent spatial-integration convolutions when learned in an incremental manner, and is further enhanced in the presence of a fully connected readout layer, suggesting that the two context mechanisms are complementary. Finally, we find that learning a receptive-field-centric model with self-attention, before incrementally learning a fully connected readout, yields a more biologically realistic model in terms of center-surround contributions.

1 Introduction

Feedforward CNN models have been shown in recent years to be an effective approach for modeling the transfer function of early visual cortical neurons to predict their responses to arbitrary natural images [12, 13, 28, 30, 3, 14]. Neurons in the primate visual cortex are known to have extensive horizontal and feedback recurrent connections for mediating contextual modulation [9, 17]. Feedforward CNNs can model the influence of contextual surround on the responses of the neurons via two mechanisms: successive convolution layers and a fully connected layer. Both can make the neural model’s responses sensitive to the global image context, outside the traditional classical receptive fields of neurons. In the context of neural prediction, it is found that including the inductive bias of horizontal recurrent connections can improve the model’s predictive capabilities [31], and that replacing a feedforward layer with a recurrent layer with a Markovian local kernel consistently outperforms the parameter-matched feedforward CNNs [10, 18, 15, 31]. However, contextual modulation in the visual cortex involves both the near surround and far surround, with the far surround being

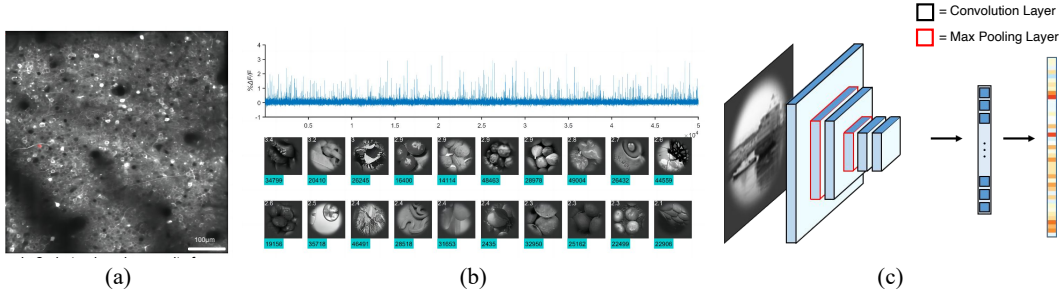


Figure 1: Macaque neuronal response dataset. **(a)** shows a two-photon image with cells. **(b)** shows the response of one neuron to 50k stimuli and the top 20 images that induced the strongest responses. On average, less than 0.5% of the images induce responses greater than half peak height. Each site contains around 300 neurons. **(c)** shows a feedforward CNN used to model neural response.

mediated by top-down feedback [1, 22, 23]. In addition, there is evidence that contextual modulation is dynamic and highly image-dependent, suggesting a flexible gating mechanism [4]. Such a flexible gating mechanism can be modeled by a combination of Gaussian mixture models, implemented either by image-dependent normalization [4] or by non-local networks and the self-attention mechanism in deep learning [8]. In this paper, we explored the benefits of introducing the inductive bias of the flexible gating mechanism using self-attention non-local networks in modeling the transfer function of neurons for predicting responses to natural images.

We found that augmenting feedforward CNNs with a self-attention non-local network layer improves two key metrics in assessing the performance of the transfer function of neurons: overall tuning correlation and prediction of the tuning peaks. To assess the relative contribution of the three contextual modulation mechanisms – convolutions, self-attention, and a fully connected readout layer – for predicting neural responses, we dissect the network by factorizing [6] the feedforward components and the three context mechanisms. We found that while the three context mechanisms complement one another to produce the best prediction performance when used in conjunction, they have specific roles. First, the fully connected layer plays a critical role in peak prediction, though self-attention can further enhance it. Second, self-attention alone can improve tuning curve correlation but is insufficient for predicting the response peak. The performance of self-attention models can be greatly enhanced when the feedforward receptive fields are learned first before learning the self-attention network, rather than learning everything simultaneously. The benefits of such incremental learning [25, 6] in this context is novel, in that it suggests that feedforward receptive fields may be learned first before the recurrent connections during the cortical development. Our findings provide insights towards the rationales underlying the computational organization, development, and selective flexibility in horizontal and feedforward connections in cortical circuits. Our work further suggests that constraining this flexibility via priors in the learning process allows for the development of a richer contextual modulation mechanism, which perhaps is useful not simply for the neural response prediction, but also more broadly for other machine learning tasks in deep learning or computer vision.

2 Related works

Modeling neural response prediction Feedforward deep neural networks have proven effective in modeling and predicting neural responses in early visual brain areas [12, 13, 28, 30, 3, 14]. However, the brain’s visual areas contain abundant recurrent connections that are essential for generating neural responses [9, 17, 24]. Incorporating biologically-inspired simple recurrent circuits, in the form of a Markov network, into convolutional neural networks has been shown to enhance efficiency compared to purely feedforward models, achieving similar performance in image classification and neural prediction tasks [31]. In the context of neural prediction, the underlying assumption is that the closer a model can replicate the neural computation mechanisms responsible for a real neuron’s response, the more accurate the model’s predictive capabilities become [20, 27, 16].

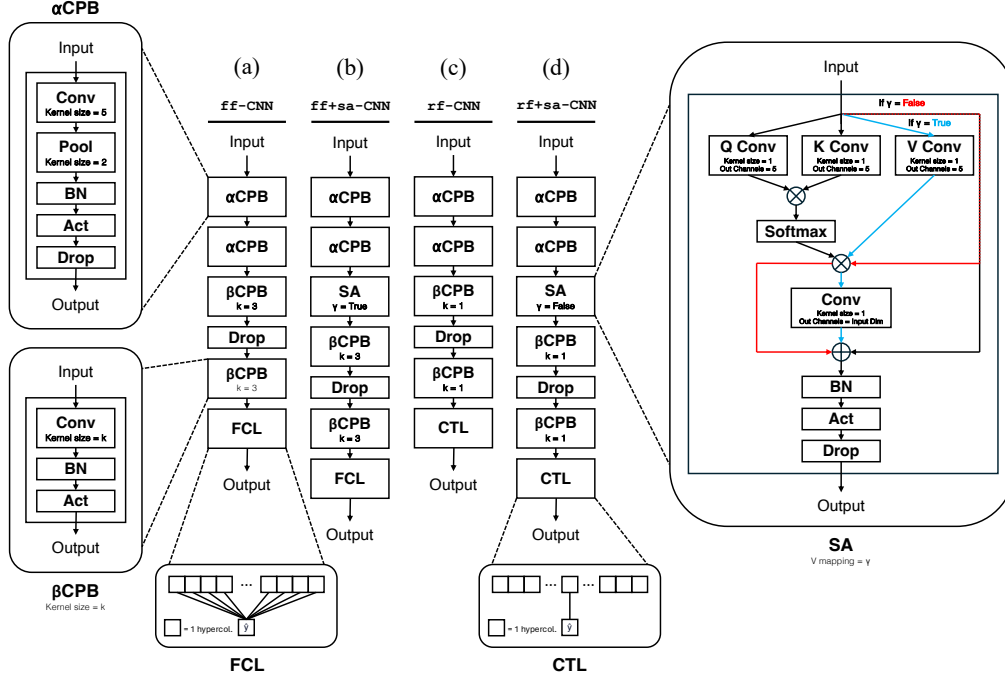


Figure 2: Models explored in this study. Models are constructed from two types of convolutional processing blocks (CPB): α CPB and β CPB. α CPB has a fixed convolution kernel size = 5 and max pooling kernel size = 2. β CPB takes an input convolution kernel size of k , and has no pooling layers. The two final layer readout modes are fully connected (FCL) and center hypercolumn only (CTL). Self-attention (SA) takes as input a boolean γ that determines whether the value (V) vector is transformed; if $\gamma = \text{True}$ then V is mapped, otherwise V is equal to the input. All models with SA utilize single-headed attention. (a) shows the feedforward CNN. (b) shows the feedforward CNN augmented with self-attention. (c) shows the receptive field CNN. (d) shows the receptive field CNN augmented with self-attention.

Self-attention for global dependencies Self-attention mechanisms have recently become a pivotal component in deep learning models, especially in natural language processing and increasingly in computer vision tasks [26, 32, 11]. In computer vision, self-attention performs a weighted average operation based on the context of input features, computing attention weights dynamically through a similarity function between pixel pairs [26, 19]. This flexibility allows the attention module to adaptively focus on different regions and capture informative features [21]. Self-attention has also been integrated with CNNs to enhance their representational power [19, 29, 2]. By enabling CNNs to consider distant spatial relationships within an image, self-attention improves the network’s ability to capture global context. This mechanism overcomes the limitations of traditional CNNs, which primarily concentrate on local features because of their convolutional structure. Taking the complementary properties of convolution and self-attention, the benefits of each paradigm can be extracted by integrating the two and using self-attention to augment convolution modules [7, 29, 19, 5].

3 Method

In this study, we developed deep learning models to model V1 neural response to natural images, with the goal of evaluating the potential roles of the self-attention mechanism in neural computation within the visual cortex. We obtained a dataset of neuronal responses measured using two-photon imaging with GCaMP5 from two awake behaving macaque monkeys performing a fixation task, consisting of 302 neurons from monkey 1 (M1S1) and 299 neurons from monkey 2 (M2S1), in response to 34k and 49k natural images extracted from the ImageNet dataset. The neurons were recorded across five days and tracked anatomically based on landmarks as well as based on their responses to 200 fingerprint images tested every day. The images were presented in sequence with 1 second per image preceded by 1 second of gray screen. The 30k-50k images in the training set were presented once,

and the 1000 images in the validation set were tested once with 10 repeats. Images were 100×100 pixels, with 30×30 pixels for 1 degree visual angle. The eccentricity of the recording sites were 3 degrees and 1.79 degrees respectively, with mean receptive fields of about 0.75 and 0.25 degrees respectively. We preprocessed the dataset before modeling, and notably downsampled input images to 50×50 pixels, yielding 15×15 pixels per degree visual angle.

3.1 Augmenting feedforward CNNs with self-attention mechanisms

Baseline feedforward model (ff-CNN) See Figure 2(a) for the architecture. ff-CNN is the baseline feedforward model for comparisons, and is comprised of two α -convolutional processing blocks (α CPB) and two β -convolutional processing blocks (β CPB), followed by a fully connected readout layer (FCL). A single ff-CNN model is fitted to each neuron. All models described below are derived from this baseline model.

Given a grayscale input image with dimensions 50×50 pixels, the two α CPB layers with a 5×5 kernel encode the input of size $(1 \times 50 \times 50)$ into $(c \times 9 \times 9)$ where $c \in \mathbb{N}$ is the number of channels ($c \in \{30, 32\}$ in this study). The center hypercolumn of the post- α CPB encoding has a centered effective receptive field size of 11×11 pixels. In other words, the center hypercolumn of the latent representation after the α CPB layers has information on the center 11×11 window of the original 50×50 input image. This window corresponds roughly to the size of the receptive field. Next, the two β CPB layers use a 3×3 kernel to further expand the effective receptive field. Finally, ff-CNN has access to the entirety of the input 50×50 image due to the final FCL readout. Thus, ff-CNN has two modalities of contextual modulation – convolutions and a fully connected layer.

Feedforward with self-attention model (ff+sa-CNN) See Figure 2(b) for the architecture. We augment ff-CNN by adding a self-attention layer immediately after the last α CPB and before the first β CPB to construct ff+sa-CNN. This placement enables SA to act on an adequately convolved feature representation, but also be further modulated by convolutions before feeding into the final layer. We compare the performance of ff+sa-CNN against that of ff-CNN, controlling the parameter counts to be roughly equal by decreasing the number of channels, which is maintained throughout entire model, from $c = 32$ in the baseline CNNs to $c = 30$ in the self-attention models to account for the addition of the SA layer. In the context of contextual modulation, ff+sa-CNN intermixes spatial interactions and inter-channel mixing across the posterior β CPB, SA, and FCL layers.

3.2 Factorizing the contextual modulation mechanisms

Next, we factorize the three context mechanisms, namely self-attention, successive convolutions, and the fully-connected layer, to evaluate their relative contributions. We first construct the rf-CNN model, which is devoid of contextual modulation, by subtracting from ff-CNN: the kernel size in the β CPB blocks are changed from 3×3 to 1×1 and the fully connected layer is changed to look only at the center hypercolumn (CTL). Then, we introduce self-attention to rf-CNN to construct rf+sa-CNN. The parameter counts are again controlled by reducing the number of channels from $c = 32$ in rf-CNN to $c = 30$ in rf+sa-CNN to compensate for the addition of the SA layer. We compare the performance of the two models, alongside the feedforward models.

Baseline receptive field model (rf-CNN) See Figure 2(c) for the architecture. Due to the 1×1 kernel size in the β CPB layers and the center hypercolumn readout layer, rf-CNN only has access to the center 11×11 of the input 50×50 image. This is because the 1×1 convolutions perform no spatial expansion before feeding into the CTL. Thus, rf-CNN is making predictions solely based on the receptive field.

Receptive field with self-attention model (rf+sa-CNN) See Figure 2(d) for the architecture. rf+sa-CNN factorizes spatial interactions and inter-channel mixing into distinct blocks. Because $v_{\text{mapping}} = \gamma = \text{False}$ in the SA layer of rf+sa-CNN, SA operates exclusively on the horizontal spatial interactions between hypercolumns without any inter-channel mixing. Furthermore, since the kernel size in rf+sa-CNN’s β CPBs are 1×1 , the β CPB layers do not convolve across different hypercolumns, and is instead equivalent to a mapping operation performed on each hypercolumn separately, or inter-channel mixing. The CTL readout layer in rf+sa-CNN forces all relevant information to be encoded in the center hypercolumn of shape $30 \times 1 \times 1$. As the baseline CNN counterpart to

rf+sa-CNN, rf-CNN, only "sees" pixels in the neuron's receptive field, the addition of SA with $\gamma = \text{False}$ effectively incorporates pixels in the surrounding portions of the image by pipelining the surround information through the center hypercolumn into the final prediction. Therefore, rf+sa-CNN has only one modality of contextual modulation – self-attention.

3.3 Incremental learning: factorizing the learning process

We factorize the training process by first learning the receptive fields of the neurons before incorporating any contextual modulation mechanisms such as self-attention and the fully connected layer. The following progression of models, rf-CNN, rf+sa-CNN*, and ff+sa-CNN* (as shown in Fig. 3), incrementally expands the capacity of contextual modulation. An important distinction between incremental models and models shown in Fig. 2, marked by *, indicates a 1×1 kernel in the β CPB, which maintain channel mixing but removes further spatial integration through convolution. rf-CNN (shown in Fig. 3(a) or Fig. 2(c)) has information only from the center receptive field. rf+sa-CNN* (shown in Fig. 3(b)) uses only the self-attention mechanism for contextual modulation. ff+sa-CNN* (shown in Fig. 3(c-d)) has the same surround-center modulation as rf+sa-CNN* from self-attention, but allows spatial integration of the global context by changing the CTL to FCL at the end. As horizontal connections in the visual cortex are known to mature after the development of the receptive fields, we designed an incremental learning setup where rf-CNN first learns the receptive fields, rf+sa-CNN* (Incr.) learns the self-attention only after the rf-CNN has already learned the receptive fields. Finally, ff+sa-CNN* (Incr.FC₁) and ff+sa-CNN* (Incr.FC₂) inherit the receptive fields and self-attention structures of rf+sa-CNN*. Models labelled (Incr.) are learned incrementally as such, and models labelled (Simul.) are traditionally trained simultaneously.

3.4 Model training and evaluation

All models were trained in PyTorch using the Adam optimizer with $\text{lr} = 0.001$ and mean squared error (MSE) loss. Hyperparameters were controlled by the validation set. Training and computations was performed on an in-house computing cluster with GPU (NVIDIA V100 or similar) nodes.

To quantify performance, models were evaluated on two criteria, Pearson correlation and peak tuning index. Pearson correlation represents the overall tuning similarity between a model's predicted responses and the real neuron's recorded responses. The peak tuning index is used to quantify how well a model can predict the strongest responses recorded by the real neuron. This lets us evaluate how well a model can discriminate between images that are strongly excitatory and images that incite a weak response.

Pearson correlation: The Pearson correlation (CORR.) is taken between neuron responses and model-predicted responses.

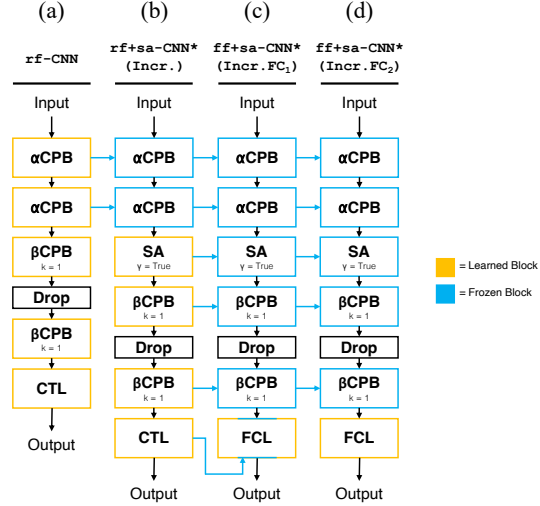


Figure 3: Incremental learning models setup. (a) shows the baseline receptive field CNN, equivalent to Fig. 2. (b) shows (a) augmented with self-attention and learned incrementally; the α CPBs are taken from (a) and the remaining layers are learned. The * denotes slight modification from rf+sa-CNN, Fig. 2(d), namely γ is changed to True. (c), (d) show the result of replacing the CTL in (b) with a FCL, and learned incrementally; (c) freezes only the center hypercolumn in the FCL (FC₁) whereas (d) allows the FCL to learn freely (FC₂). (c) and (d) have all other layers taken from (b). The * denotes slight modification from ff+sa-CNN, Fig. 2(b), namely k in β CPB is changed to $k = 1$. (Simul.) models are equivalent in architecture, except all blocks are learned.

Peak tuning index: The peak tuning index (PT) is a membership metric of the strongest predictions above a threshold determined by the top 1% of real responses. PT can be interpreted as the percentage of the peak that a model captures. The index is calculated as:

$$PT = \frac{\# \text{ of top 1\% predictions } \geq \min(\text{top 1\% real responses})}{\# \text{ of responses in the top 1\%}} \times 100\%$$

PT is divided into PT_J and PT_S , based on how the top 1% predictions is defined. PT_J is when predictions are jointly rank ordered with respect to the real responses. PT_S is when predictions are separately rank ordered independently of the real responses. PT_J is a stricter measure. Note that because we train with MSE loss, models are incentivized to minimize the absolute difference between predictions and real responses, rather than match the curvature of the tuning curve. This minimizes the risk of PT being misrepresentative due to lateral shifts in the tuning curve.

4 Results

4.1 Self-attention CNN models outperform parameter-matched CNN models

To gauge the efficacy of self-attention in modeling horizontal interactions, we compared self-attention CNNs to their parameter-matched CNN counterparts (see Fig. 2). Both self-attention models had higher Pearson correlations than the baseline ff-CNN (see Table 1).

Comparing ff-CNN and ff+sa-CNN reveals that incorporating SA as an additional structure to integrate horizontal connections improves prediction accuracy. ff-CNN has access to the entire image through receptive field expansion via convolutions, and a fully connected readout layer that incorporates all spatial dependencies. Adding SA as a further mode of surround integration in ff+sa-CNN proves beneficial. However, due to the integrated interactions between feed-forward and horizontal operations in ff-CNN and ff+sa-CNN, it is difficult to dissect the exact importance of each model component.

To address this, we tested models that factorized feed-forward and horizontal interactions. Comparing ff-CNN and rf+sa-CNN shows that separating spatial and column-wise interactions into SA and 1×1 convolutions under a center hypercolumn readout is better at modeling overall tuning than having joint interactions within 3×3 convolutions and a fully connected readout. Furthermore, because rf+sa-CNN and ff+sa-CNN have similar correlations, factorizing interactions is as effective as integrating interactions in the presence of a SA block.

We notably observed that rf-CNN had the highest correlation, suggesting that basing predictions solely on the center receptive field yields the best overall tuning.

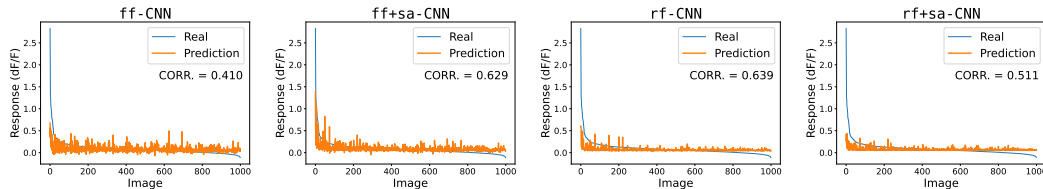


Figure 4: Tuning curve and Pearson correlation for models. Despite rf-CNN having the largest correlation, it is clear that ff+sa-CNN is able to capture peak tuning significantly better, at the cost of a noisier overall tuning. Example shown is M1S1 neuron 238. See A.4 for population averages.

Pearson correlation, however, is not a holistic measure of similarity in behavior between models and real neurons. Juxtaposing the tuning curves for each model reveals that despite improved correlations in rf-CNN, ff+sa-CNN, and rf+sa-CNN, the models have varying peak prediction heights that follow different trends (example shown in Fig. 4).

Table 1: Average Pearson correlation for models trained on M1S1 and M2S1. SEM = 0.009 was consistent across models and monkeys.

| Model | M1S1 | | M2S1 | |
|-----------|--------------|-----------------|--------------|-----------------|
| | CORR. | Δ ff-CNN | CORR. | Δ ff-CNN |
| ff-CNN | 0.393 | 0.0% | 0.477 | 0.0% |
| ff+sa-CNN | 0.416 | +6.6% | 0.491 | +3.3% |
| rf-CNN | 0.420 | +8.6% | 0.496 | +4.3% |
| rf+sa-CNN | 0.414 | +7.2% | 0.486 | +2.4% |

4.2 Surround information is important for peak tuning

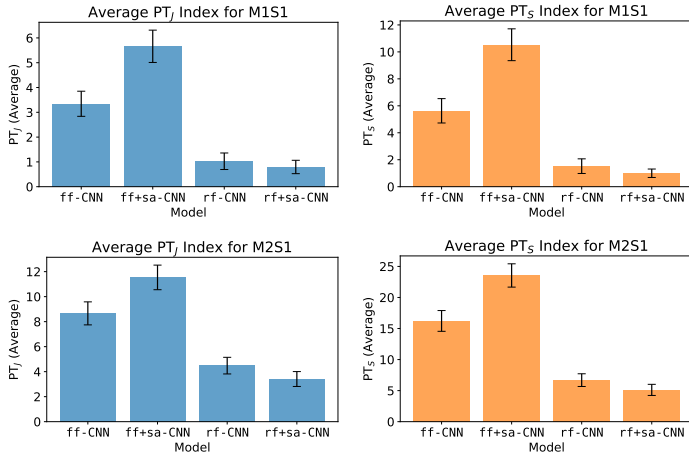


Figure 5: Average peak tuning indices for models. **Top row:** bar charts for M1S1. **Bot row:** bar charts for M2S1. **Left col:** average PT_J values. **Right col:** average PT_S values. Error bars are SEM. Models with integrated surround and inter-channel interactions (ff-CNN and ff+sa-CNN) were able to predict the peak better than models that factorized the two (rf+sa-CNN) or had no surround interactions at all (rf-CNN). This is supported by both PT_J and PT_S values (as shown in Fig. 5).

Models with integrated interactions predicted peak responses the best, despite models with factorized interactions or no surround interactions having a better correlation. This suggests that the 3×3 convolution and fully connected readout are most important for capturing the strongest real responses, compared to the 1×1 convolution and center hypercolumn readout. Therefore, surround information plays a pivotal role in capturing the tuning peak. In the context of a 3×3 convolution and FCL, we observe that SA provides a significant improvement to peak tuning, as demonstrated by the comparison between ff-CNN and ff+sa-CNN.

Counter-intuitively, however, rf+sa-CNN had lower PT_J and PT_S values compared to rf-CNN, as well as a lower correlation. This means that the addition of self-attention was detrimental to performance. Moreover, this comparison implies that making predictions based only on the receptive field is superior to incorporating surround information into the receptive field representation using self-attention.

4.3 Incremental learning outperforms traditional training methods

Motivated by the poor peak tuning of rf+sa-CNN compared to rf-CNN (see Fig. 5), we conducted an incremental training experiment where models were forced to learn the receptive field first, before incorporating surround information (setup described in Fig. 3). Effectively, we have factorized the learning process for each model (in addition to feed-forward and horizontal interactions within each model) into the center, followed by the surround.

Table 2: Average Pearson correlation for models incrementally and simultaneously trained on M1S1 and M2S1. SEM = 0.009 was consistent across models and monkeys.

| Model (Training Method) | M1S1 | | M2S1 | |
|-----------------------------------|--------------|-----------------|--------------|-----------------|
| | CORR. | Δ rf-CNN | CORR. | Δ rf-CNN |
| rf-CNN(Simul.) | 0.420 | 0.0% | 0.496 | 0.0% |
| rf+sa-CNN*(Simul.) | 0.409 | -2.6% | 0.480 | -3.2% |
| rf+sa-CNN*(Incr.) | 0.421 | +0.6% | 0.493 | -0.3% |
| ff+sa-CNN*(Simul.) | 0.416 | -0.8% | 0.490 | -0.7% |
| ff+sa-CNN*(Incr.FC ₁) | 0.430 | +3.0% | 0.494 | -0.1% |
| ff+sa-CNN*(Incr.FC ₂) | 0.414 | -1.3% | 0.488 | -1.1% |

While rf-CNN significantly outperformed rf+sa-CNN in both correlation (see Table 2) and peak tuning (see Fig. 6), we observed that rf+sa-CNN*(Incr.) performed similarly to rf-CNN in both aspects. rf+sa-CNN*(Incr.)’s simultaneously trained counterpart, rf+sa-CNN*(Simul.), produced a similar drop in performance from rf-CNN as rf+sa-CNN did. rf+sa-CNN*(Incr.) also outperformed rf+sa-CNN*(Simul.) in both correlation and peak tuning. Thus, in a factorized model, learning to process the neuron’s receptive field first before considering any surround informa-

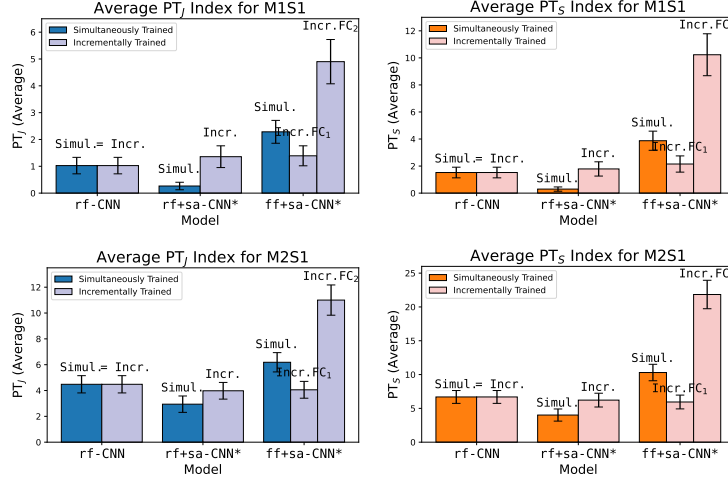


Figure 6: Average peak tuning indices for incrementally and simultaneously trained models. **Top row:** bar charts for M1S1. **Bot row:** bar charts for M2S1. **Left col:** average PT_J values. **Right col:** average PT_S values. Error bars are SEM.

tion is superior to trying to do both simultaneously. Furthermore, self-attention, when configured with a CTL readout, is not a sufficient mechanism in capturing the tuning peak on its own.

All $ff+sa-CNN^*$ models saw an improvement in PT_J and PT_S over all $rf+sa-CNN^*$ models. This indicates that either the FCL layer is the most important factor in predicting peak responses, or that constraining the readout to CTL in $rf+sa-CNN^*$ does not allow for adequate error propagation to the self-attention block during training, causing self-attention to be poorly learned and preventing performance improvements.

Comparing the peak tuning of $ff+sa-CNN^*(Incr.FC_2)$ to $ff+sa-CNN^*(Simul.)$, we conclude that by first fixating the center receptive field from $rf-CNN$ and surround modulation on the center from $rf+sa-CNN^*(Incr.)$, and then aggregating all spatial information through the FCL, we can greatly improve the peak performance. Thus, using a guided learning approach with upstream fixation and downstream flexibility allows us to achieve performance similar to the $ff+sa-CNN$ (performance shown in Table 1 and Fig. 5), when the model would have been otherwise much more limited if learned simultaneously ($ff+sa-CNN^*(Simul.)$). Note that the only difference between $ff+sa-CNN$ and $ff+sa-CNN^*$ is a 3×3 versus 1×1 in the βCPB layers, respectively. This means that we do not need to rely on convolution for spatial integration after the self-attention layer for modeling these neurons if we train the model incrementally.

Now, if we instead elect to fixate modules both upstream and downstream as in $ff+sa-CNN^*(Incr.FC_1)$, and learn only the surround information in the FCL (the center hypercolumn contribution is fixed), we observe a weaker peak tuning compared to the same model trained simultaneously, but a much stronger correlation. Because we’ve fixated the center contribution from $rf+sa-CNN^*(Incr.)$, a model that funnels all information into the center hypercolumn, this result is consistent with the idea that the center receptive field is important for overall tuning, whereas the allowing for surround-center integration is important for the tuning peak.

4.4 Incremental learning emphasizes the contribution of the classical receptive field

When we decompose the center and surround contributions to the final prediction from the hypercolumns in the FCL, we observe that in $ff+sa-CNN^*(Incr.FC_2)$ the center is the primary constituent (as shown in Fig. 7). We further find that the surround selectively strengthens the prediction in the cases where the center is already strong, providing evidence that the surround is directly critical for peak tuning. These effects are not seen in $ff+sa-CNN^*(Simul.)$. When we train the model simultaneously, the center hypercolumn is not learned to become the strongest constituent. Instead, the contributions from the hypercolumns become evenly dispersed.

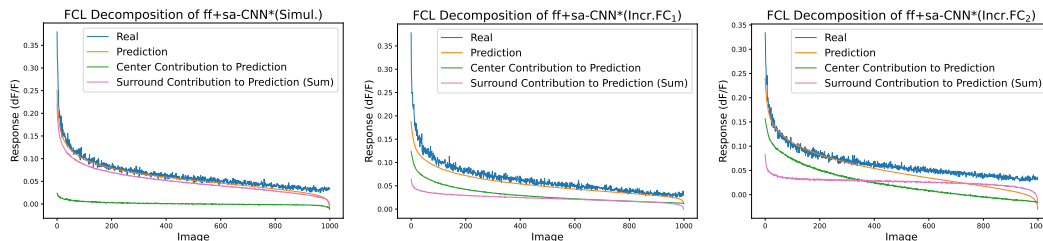


Figure 7: Average FCL decomposition of $\text{ff}+\text{sa}-\text{CNN}^*$ when trained differently. The center contribution (green) and the total surround contribution (pink) sum to the prediction tuning curve (orange). Plots are rank ordered with respect to predicted responses. Averages are calculated by plotting rank ordered decomposed tuning curve for each neuron, then averaging across each image number. Individual contributions from hypercolumns can be found in A.5.

Although $\text{ff}+\text{sa}-\text{CNN}^*(\text{Incr. FC}_2)$ has the freedom to weigh the contributions of each hypercolumn in the final layer freely, we observed that incremental learning incentivizes the center hypercolumn to be the major contributor to the response prediction, and allows the surround to modulate the center. The same model learned simultaneously, however, learned an evenly distributed contribution across hypercolumns, with the receptive field center playing a far smaller role, in contrast to biology (Fig. 7).

5 Discussion

In this paper, we analyzed the incorporation of the self-attention mechanism into existing deep-learning models of cortical neurons. Self-attention resembles the three-way interactions found in probabilistic graphical models, allowing for center-surround interactions to be modulated by contextual variables, which can implement the flexible gating mechanism for modeling V1 neural responses [4, 8]. There are a number of interesting findings in this work that illuminate our understanding of cortical computation and neural codes. First, surround information is necessary for strong peak tuning. Although $\text{rf}-\text{CNN}$ produced the highest Pearson correlation (see Table 1) for the overall neuronal tuning curves of the neurons, incorporation of surround information using at least two of the three contextual modulation mechanisms (convolutions, self-attention, or fully connected readout) is critical in modeling the neurons' tuning peaks (see Fig. 5). This suggests the peak tuning of many V1 neurons involves recurrent circuits and contextual processing. Second, convolutional expansion of the receptive field as a context mechanism, i.e. the βCPB layers with 3×3 kernels, is not critical. Their contributions can be replaced by the self-attention mechanism learned incrementally (see $\text{ff}+\text{sa}-\text{CNN}$ in Fig. 5 versus $\text{ff}+\text{sa}-\text{CNN}^*(\text{Incr. FC}_2)$ in Fig. 6). Third, feedforward CNNs augmented with self-attention, particularly when trained incrementally, provide better performing and "biologically realistic" models. Traditionally trained self-attention models improve overall tuning (see $\text{ff}+\text{sa}-\text{CNN}$ in Table 1 and $\text{ff}+\text{sa}-\text{CNN}^*(\text{Simul.})$ in Table 2), but display evenly distributed contributions from the center and surround in the FCL fully connected layer (see $\text{ff}+\text{sa}-\text{CNN}^*(\text{Simul.})$ in Fig. 7). Incrementally trained self-attention models learn to strongly emphasize receptive field contributions over surround contributions, even when the contribution weights from the RF center hypercolumn are not frozen (see $\text{ff}+\text{sa}-\text{CNN}^*(\text{Incr. FC}_1)$ and $\text{ff}+\text{sa}-\text{CNN}^*(\text{Incr. FC}_2)$ in Fig. 7). Finally, self-attention standalone is not self-sufficient for capturing peak responses; rather, it serves as a complementary mechanism that bolsters the fully connected readout, which is the critical factor for peak tuning (see Fig 5 and Fig. 6). This may be because SA is primarily modifying only the center hypercolumn using three-way interactions, whereas FCL has fuller access to surrounding information and can integrate them explicitly. We further observed that models that can capture peak tuning exhibit interpretable contextual modulation, such as association fields, in the self-attention module (see A.6). Self-attention models also prove to be more data efficient (see A.7). A limitation of our work is that we do not fully understand the nature of the complementary interaction between self-attention and the fully connected layer in integrating contextual information. Further theoretical and experimental studies are required to characterize these interactions and understand how they are implemented by biological circuits.

Broader impacts and ethics statement Animal experiments involved in this study advance our understanding of the neural codes in the brain, and all procedures have been approved by the institutional animal care and use committee. This is a computational neuroscience study investigating self-attention and CNNs for modeling neurons, which is important for understanding neural codes and neural processing in the brain. The results may contribute towards the development of more powerful artificial intelligence (AI) and deep learning models. While advancing AI can yield both positive and negative societal impacts, furthering our collective understanding of deep learning and neuroscience is essential for countering misuse by malicious actors in this technological race.

References

- [1] Alessandra Angelucci and Paul C. Bressloff. Contribution of feedforward, lateral and feedback connections to the classical receptive field center and extra-classical receptive field surround of primate v1 neurons. In S. Martinez-Conde, S.L. Macknik, L.M. Martinez, J.-M. Alonso, and P.U. Tse, editors, *Visual Perception*, volume 154 of *Progress in Brain Research*, pages 93–120. Elsevier, 2006.
- [2] Irwan Bello, Barret Zoph, Ashish Vaswani, Jonathon Shlens, and Quoc V. Le. Attention augmented convolutional networks, 2020.
- [3] Santiago A. Cadena, George H. Denfield, Edgar Y. Walker, Leon A. Gatys, Andreas S. Tolias, Matthias Bethge, and Alexander S. Ecker. Deep convolutional models improve predictions of macaque v1 responses to natural images. 2017.
- [4] Ruben Coen-Cagli, Adam Kohn, and Odelia Schwartz. Flexible gating of contextual influences in natural vision. *Nature neuroscience*, 18, 10 2015.
- [5] Jean-Baptiste Cordonnier, Andreas Loukas, and Martin Jaggi. On the relationship between self-attention and convolutional layers, 2020.
- [6] R. James Cotton, Fabian H. Sinz, and Andreas S. Tolias. Factorized neural processes for neural processes: k -shot prediction of neural responses, 2020.
- [7] Zihang Dai, Hanxiao Liu, Quoc V. Le, and Mingxing Tan. Coatnet: Marrying convolution and attention for all data sizes, 2021.
- [8] Yicheng Fei and Xaq Pitkow. Attention as inference with third-order interactions. In *NeurIPS '22 Workshop on All Things Attention: Bridging Different Perspectives on Attention*, 2022.
- [9] Daniel J. Felleman and David C. van Essen. Distributed hierarchical processing in the primate cerebral cortex. *Cerebral cortex*, 1 1:1–47, 1991.
- [10] Kuan Han, Haiguang Wen, Yizhen Zhang, Di Fu, Eugenio Culurciello, and Zhongming Liu. Deep predictive coding network with local recurrent processing for object recognition, 2018.
- [11] Kyungmin Kim, Bichen Wu, Xiaoliang Dai, Peizhao Zhang, Zhicheng Yan, Peter Vajda, and Seon Kim. Rethinking the self-attention in vision transformers. In *2021 IEEE/CVF Conference on Computer Vision and Pattern Recognition Workshops (CVPRW)*, pages 3065–3069, 2021.
- [12] William F. Kindel, Elijah D. Christensen, and Joel Zylberberg. Using deep learning to probe the neural code for images in primary visual cortex. *Journal of Vision*, 19(4):29–29, 04 2019.
- [13] David A. Klindt, Alexander S. Ecker, Thomas Euler, and Matthias Bethge. Neural system identification for large populations separating "what" and "where", 2018.
- [14] Nikolaus Kriegeskorte. Deep neural networks: A new framework for modeling biological vision and brain information processing. *Annual Review of Vision Science*, 1(Volume 1, 2015):417–446, 2015.
- [15] Jonas Kubilius, Martin Schrimpf, Kohitij Kar, Ha Hong, Najib J. Majaj, Rishi Rajalingham, Elias B. Issa, Pouya Bashivan, Jonathan Prescott-Roy, Kailyn Schmidt, Aran Nayebi, Daniel Bear, Daniel L. K. Yamins, and James J. DiCarlo. Brain-like object recognition with high-performing shallow recurrent anns, 2019.
- [16] Zhe Li, Wieland Brendel, Edgar Y. Walker, Erick Cobos, Taliah Muhammad, Jacob Reimer, Matthias Bethge, Fabian H. Sinz, Xaq Pitkow, and Andreas S. Tolias. Learning from brains how to regularize machines, 2019.
- [17] Nikola T. Markov, Julien Vezoli, Pascal Chameau, Arnaud Falchier, René Quilodran, Cyril Huissoud, Camille Lamy, Pierre Misery, Pascale Giroud, Shimon Ullman, Pascal Barone, Colette Dehay, Kenneth Knoblauch, and Henry Kennedy. Anatomy of hierarchy: Feedforward and feedback pathways in macaque visual cortex. *Journal of Comparative Neurology*, 522(1):225–259, 2014.
- [18] Aran Nayebi, Daniel Bear, Jonas Kubilius, Kohitij Kar, Surya Ganguli, David Sussillo, James J. DiCarlo, and Daniel L. K. Yamins. Task-driven convolutional recurrent models of the visual system, 2018.
- [19] Xuran Pan, Chunjiang Ge, Rui Lu, Shiji Song, Guanfu Chen, Zeyi Huang, and Gao Huang. On the integration of self-attention and convolution, 2022.

- [20] Galen Pogoncheff, Jacob Granley, and Michael Beyeler. Explaining v1 properties with a biologically constrained deep learning architecture, 2023.
- [21] Prajit Ramachandran, Niki Parmar, Ashish Vaswani, Irwan Bello, Anselm Levskaya, and Jonathon Shlens. Stand-alone self-attention in vision models, 2019.
- [22] Kosei Sasaki, Elizabeth C. Cropper, Klaudiusz R. Weiss, and Jian Jing. Functional differentiation of a population of electrically coupled heterogeneous elements in a microcircuit. *Journal of Neuroscience*, 33(1):93–105, 2013.
- [23] S. Shushruth, Lauri Nurminen, Maryam Bijanzadeh, Jennifer M. Ichida, Simo Vanni, and Alessandra Angelucci. Different orientation tuning of near- and far-surround suppression in macaque primary visual cortex mirrors their tuning in human perception. *The Journal of Neuroscience*, 33:106 – 119, 2013.
- [24] Courtney J Spoerer, Tim C Kietzmann, Johannes Mehrer, Ian Charest, and Nikolaus Kriegeskorte. Recurrent neural networks can explain flexible trading of speed and accuracy in biological vision. *bioRxiv*, 2020.
- [25] Gido van de Ven, Tinne Tuytelaars, and Andreas Tolias. Three types of incremental learning. *Nature Machine Intelligence*, 4:1–13, 12 2022.
- [26] Ashish Vaswani, Noam Shazeer, Niki Parmar, Jakob Uszkoreit, Llion Jones, Aidan N. Gomez, Lukasz Kaiser, and Illia Polosukhin. Attention is all you need, 2023.
- [27] Konstantin F. Willeke, Kelli Restivo, Katrin Franke, Arne F. Nix, Santiago A. Cadena, Tori Shinn, Cate Nealley, Gabrielle Rodriguez, Saumil Patel, Alexander S. Ecker, Fabian H. Sinz, and Andreas S. Tolias. Deep learning-driven characterization of single cell tuning in primate visual area v4 unveils topological organization. *bioRxiv*, 2023.
- [28] Daniel Yamins and James J. DiCarlo. Using goal-driven deep learning models to understand sensory cortex. *Nature Neuroscience*, 19:356–365, 2016.
- [29] Baosong Yang, Longyue Wang, Derek Wong, Lidia S. Chao, and Zhaopeng Tu. Convolutional self-attention networks, 2019.
- [30] Yimeng Zhang, Tai Sing Lee, Ming Li, Fang Liu, and Shiming Tang. Convolutional neural network models of v1 responses to complex patterns. *Journal of Computational Neuroscience*, 46:33 – 54, 2018.
- [31] Yimeng Zhang, Harold Rockwell, Sicheng Dai, Ge Huang, Stephen Tsou, Yuanyuan Wei, and Tai Sing Lee. Recurrent networks improve neural response prediction and provide insights into underlying cortical circuits, 2022.
- [32] Hengshuang Zhao, Jiaya Jia, and Vladlen Koltun. Exploring self-attention for image recognition, 2020.

A Appendix

A.1 V mapping parameter γ in self-attention

In the self-attention layer (as shown in Fig. 2), the V mapping parameter γ allows further factorization of inter-channel mixing and spatial interactions. Toggling $\gamma = \text{False}$ removes the transformed value vector, and attention weights instead directly on the input representation. Note that the γ parameter does make a difference performance wise. The only difference between rf+sa-CNN^* and rf+sa-CNN is the presence of a SA with $\gamma = \text{True}$ block in the former and a SA with $\gamma = \text{False}$ block in the latter. rf+sa-CNN^* has better correlation, PT_J , and PT_S values, meaning allowing for the V mapping in SA allows for more flexibility, despite the lack of a 3×3 convolution and FCL layer in these models.

A.2 CTL channel number bottleneck

In models with a CTL readout, the final layer is performing a 30 to 1 or 32 to 1 weighted sum, depending on the number of channels. Thus, an issue we considered was that such a narrow final layer would inhibit proper backpropagation of error signals to upstream modules. To address the concern of a $30 \rightarrow 1$ mapping in the CTL layer being too tight of an initial bottleneck, we trained rf+sa-CNN with $c = 375$ channels, so that it would have a $375 \rightarrow 1$ CTL mapping instead. The results were comparable to the rf+sa-CNN with $c = 30$, meaning the drop in performance from rf-CNN cannot be attributed to a parameter bottleneck.

A.3 Importance of post-self-attention channel mixing

Additionally, we tested self-attention models without post-SA convolutions (i.e. no βCPB layers) and observed sharp drops in performances compared to baseline CNNs. This suggests that inter-channel mixing is crucial in processing the output of self-attention into an interpretable representation by the readout layer. We note that transformer block in modern computer vision models employ a multi-layer perceptron immediately after self-attention, which aligns with our findings.

To compare the importance of the 3×3 versus 1×1 kernel size and FCL vs CTL readout as a means of incorporating surround information, we compared the following models: $[\alpha\text{CPB} \rightarrow \alpha\text{CPB} \rightarrow \text{SA}(\gamma = \text{True}) \rightarrow \beta\text{CPB}(k = 1) \rightarrow \beta\text{CPB}(k = 1) \rightarrow \text{FCL}] \overset{\text{vs}}{\longleftrightarrow} [\alpha\text{CPB} \rightarrow \alpha\text{CPB} \rightarrow \text{SA}(\gamma = \text{True}) \rightarrow \beta\text{CPB}(k = 3) \rightarrow \beta\text{CPB}(k = 3) \rightarrow \text{CTL}]$.

The former with $\beta\text{CPB}(k = 1)$ and FCL outperformed the latter with $\beta\text{CPB}(k = 3)$ and CTL. Thus, direct access to all spatial features with a fully connected layer is stronger than convolving the surround into the center. We observe that the FCL is the strongest factor for predicting the peak responses, and is bolstered by the addition SA, as ff+sa-CNN outperforms ff-CNN in peak tuning.

A.4 Performance of different models in predicting population tuning curves

Differences in peak tuning can also be observed in the population tuning curves (see Fig. 8). Average curves are derived by calculating rank ordered tuning curves for each neuron individually, then averaging over the image number across neurons.

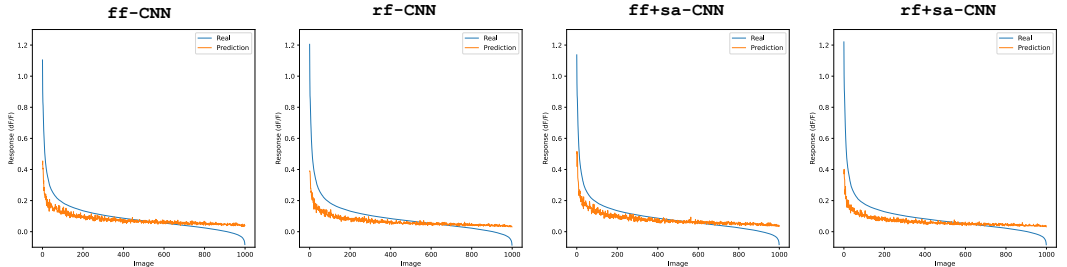


Figure 8: Population average tuning curves for M1S1.

A.5 FCL decomposition: average contribution from each hypercolumn

Fig. 7 plots the individual contribution of the center hypercolumn with the sum of all surrounding hypercolumns. We observed an evenly distributed contribution from all hypercolumns in the simultaneously trained model, but a strong center contribution in incrementally learned models. This effect is further observed when we display the average contribution of each hypercolumn (see Fig 9).

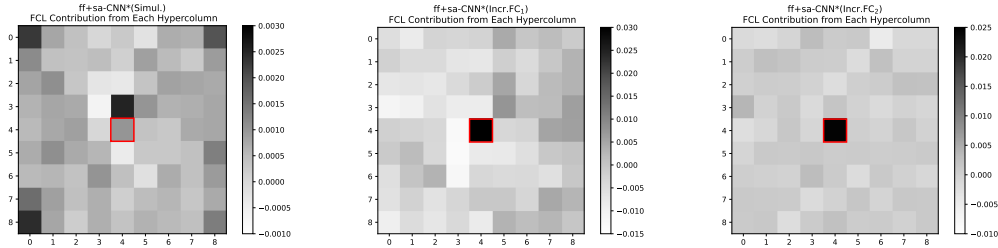


Figure 9: Average FCL contribution from each hypercolumn for MIS1. Center hypercolumn outlined in red. Each heatmap is independently contrast normalized. Note that the distribution in the first heatmap is evenly distributed compared to the others (see contrast scale).

A.6 Models that can capture peak tuning exhibit interpretable contextual modulation such as association fields in the self-attention module

Comparing the attention highlighting between self-attention models from the incremental learning experiment, we observe that models learned incrementally have a more focused attention versus equivalent-architecture counterparts trained simultaneously (as shown in Fig. 10). Models with strong peak tuning, which incorporate the surround properly, displays association field effects, focusing on similar patterns as present in the receptor field. Furthermore, because of the incremental freezing scheme between all incremental models, they have the same attention despite variations in the readout layer. However, incremental models display a focused attention, meaning the initially trained SA representation using the CTL (in $rf+sa-CNN^*(Incr)$) allows for proper learning of attention weights. This further supports that the 30 to 1 parameter bottleneck in the CTL is not a limiting factor, and the the gain in performance in the latter incremental models (in $ff+sa-CNN^*(Incr.FC_1)$ and $ff+sa-CNN^*(Incr.FC_2)$) are associated with the FCL.

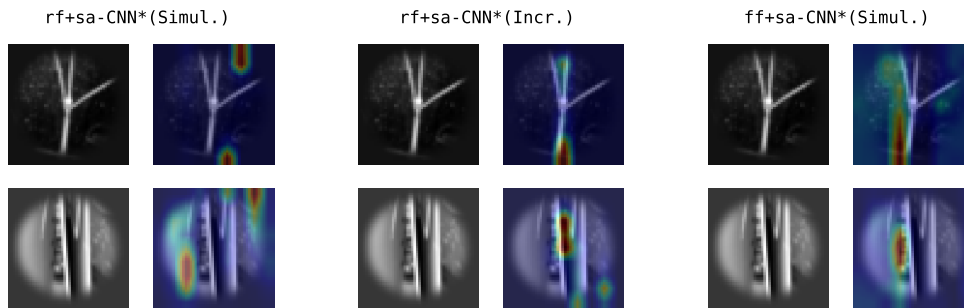


Figure 10: Attention highlighting for incremental learning models. Top two highest response inducing image are shown for MIS1 neuron 153. Note that $rf+sa-CNN^*(Incr)$, $ff+sa-CNN^*(Incr.FC_1)$, and $ff+sa-CNN^*(Incr.FC_2)$ all have the same attention map due to the freezing scheme. The center hypercolumn is queried for highlighted images.

A.7 Self-attention CNNs are data efficient

We trained baseline feedforward CNN models and their counterparts with self-attention at various training dataset sizes. We conclude that percentage improvements over `ff-CNN` are furthered at lower data constraints (as shown in Table 3), alluding to the potential efficiency of SA in accumulating surround information compared to other context mechanisms.

Table 3: Average Pearson correlation for models trained at different data sizes of M1S1. SEM = 0.008 was consistent across models.

| Model | 25% of M1S1 | | | 50% of M1S1 | | |
|------------------------|---------------------------------------|--------|--------|---------------------------------------|--------|--------|
| | Δ CORR. of <code>ff-CNN</code> | PT_J | PT_S | Δ CORR. of <code>ff-CNN</code> | PT_J | PT_S |
| <code>ff-CNN</code> | 0.0% | 0.232 | 1.026 | 0.0% | 0.762 | 1.556 |
| <code>ff+sa-CNN</code> | +7.2% | 0.927 | 1.656 | +7.6% | 1.026 | 2.715 |
| <code>rf-CNN</code> | +26.9% | 0.000 | 0.000 | +21.1% | 0.000 | 0.000 |
| <code>rf+sa-CNN</code> | +23.6% | 0.000 | 0.000 | +19.8% | 0.000 | 0.000 |

A.8 Code for experiments

The code is hosted at the github repository: <https://anonymous.4open.science/r/sacnn/>